A novel mechanism of heme degradation to biliverdin studied by QM/MM and QM calculations

Alavi, Fatemeh Sadat; Gheidi, Mahin; Zahedi, Mansour; Safari, Nasser; Ryde, Ulf

Published in:
Dalton Transactions

DOI:
10.1039/c8dt00064f

2018

Document Version:
Peer reviewed version (aka post-print)

Novel Mechanism of Heme Degradation to Biliverdin Studied by QM/MM and QM Calculations

Fatemeh Sadat Alavi[a],Mahin Gheidi[a], Mansour Zahedi[a,*], Nasser Safari[a,*], Ulf Ryde[b]

[a]Department of Chemistry, Faculty of Sciences, Shahid Beheshti University, G.C., Evin, 19839-6313, Tehran, Iran, [b]Department of Theoretical Chemistry, Lund University, Chemical Centre, P.O. Box 124,SE-221 00 Lund, Sweden

Abstract

Heme degradation by heme oxygenase enzymes is important for maintaining iron homeostasis and prevention of oxidative stress. Previous studies have reported that heme degradation proceeds through three consecutive steps of O_2 activation: the regiospecific self-hydroxylation of heme, conversion of hydroxyheme to verdoheme and CO, and the cleavage of verdoheme macrocycle to release biliverdin and free ferrous iron. Our results indicate that in the second step of heme degradation, not only verdoheme is generated but ring opening and biliverdin production can also occur. We have performed QM-cluster and QM/MM calculations, which show that calculations with H_2O as the axial ligand of Fe give the lowest barrier. In the QM-cluster calculation, the reaction is exothermic by –85 kcal/mol and the rate-limiting barrier is 5 kcal/mol, whereas the corresponding QM/MM calculations give a slightly lower barrier of 3 kcal/mol, owing to strong hydrogen bonds and the protein environment.

Introduction

Heme oxygenases (HOs) are important enzymes that are involved in the recycling of heme iron and generation of the neurotransmitter CO molecule and biliverdin as a defense mechanism against oxidative stress.[1-7] Extensive previous studies have established that the reaction catalyzed by HO proceeds through at least three steps. The first step is the oxidation of heme to α-meso-hydroxyheme.[8] In the second step, α-meso-hydroxyheme is converted into verdoheme and CO.[9]

In the third step, biliverdin is formed from verdoheme, concomitantly with release of Fe^{2+}[10] (see Scheme 1).[11, 12]

Scheme 1. The three-step degradation of heme catalyzed by HO.

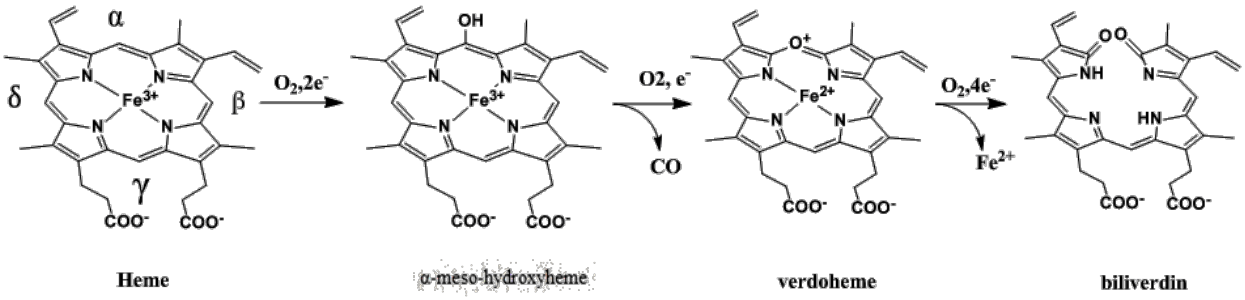

In this paper, we propose a new heme cleavage mechanism, suggesting that whereas a five-coordinated hydroxyheme may form verdoheme when it reacts with O_2[13, 14], if the Fe ion binds the released CO molecule or water as the sixth ligand, the reaction with O_2 instead leads to ring opening and biliverdin production. Thus, both biliverdin and verdoheme production can occur simultaneously, which is corroborated by experimental evidence.[15]

Since the first step, in which the heme is converted to α-meso-hydroxyheme by hydroxylation of the α-meso position, is regioselective and governing the follow-up reactions, it has been studied extensively.[16] Pervious density functional theory (DFT) calculations have suggested that iron (III) hydroxyheme is converted to iron(III) superoxo oxophlorin in the presence of dioxygen. Three major resonances form of hydroxyheme or oxophlorin has been suggested by our group[17, 18] (see Scheme3). The reactivity of these isoforms depends on electronic environment and iron coordination. The oxophlorin ring has a radical nature with spin delocalization on the oxygen and meso carbon adjacent to it. This electronic and spin delocalization on the ring is key to the reactivity of the ring toward dioxygen and the main reactive form is the neutral keto π-radical resonance structure.

In addition, our previous studies showed[18] that the binding of H_2O, O_2 or CO to the Fe ion in iron oxophlorin will shift the electronic structure toward the neutral keto π-radical resonance form in the following order: $CO>O_2>H_2O$.

Five-coordinated oxophlorin can be attacked by O_2 at two sites. It can either bind to the iron ion or it can attack the carbon atom adjacent to the carbonyl group. Since iron has a high positive charge, the former possibility is 35 kcal/mol more favorable than the second one.[13, 14] Previous QM and QM/MM studies has shown that Fe-coordinated O_2 can react with the heme ring, resulting in the formation of verdoheme.[13, 14] However, if the sixth position of the iron ion is occupied with another molecule (e.g. CO, H_2O or O_2; H2O and O_2 are available in the enzyme environment and CO is formed during the conversion of the oxophlorin to verdoheme), O_2 may react differently, yielding instead biliverdin. (Shown in Scheme 2)

Scheme 2. The proposed heme degradation catalyzed pathway.

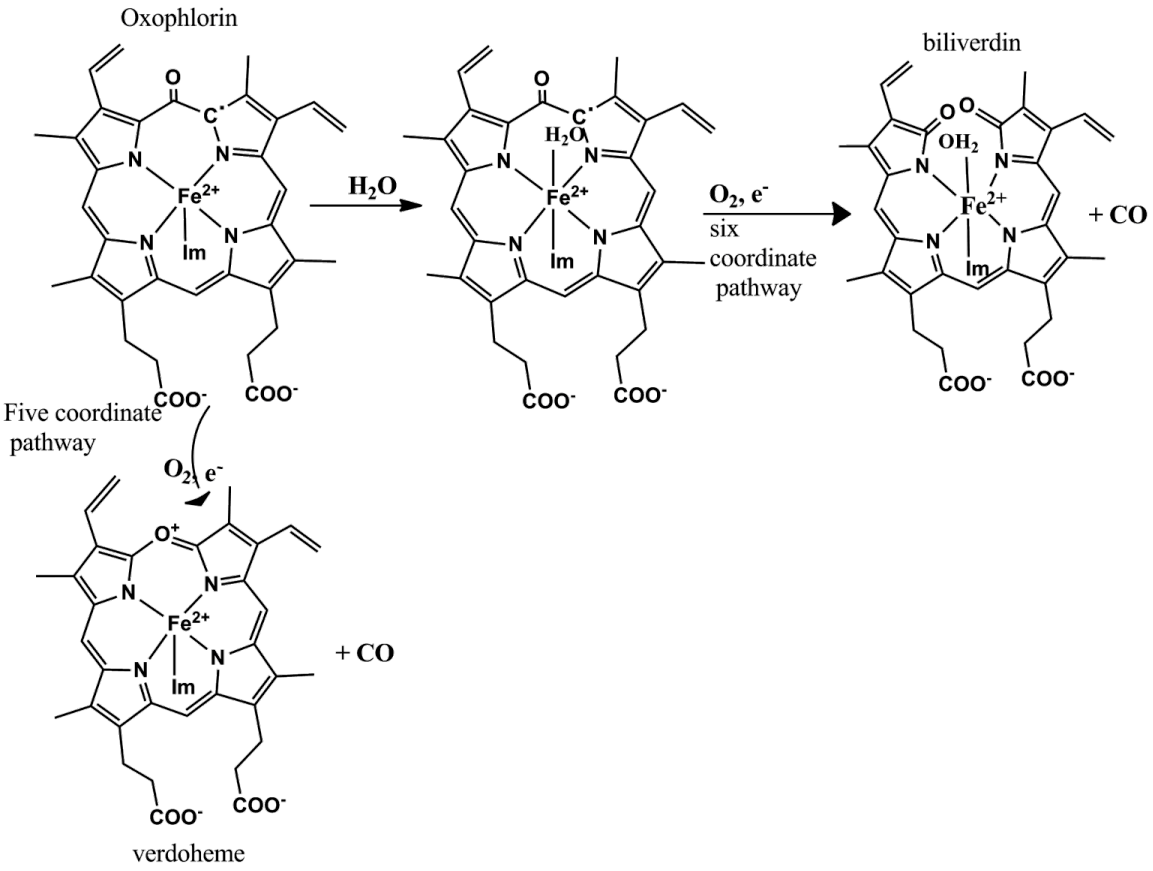

Despite various efforts to explain the second and third steps of the heme cleavage mechanism, it is apparent that there are still significant discrepancies among the mechanism proposed by the theoretical results and those from the experimental studies.[10, 13, 15]

During the last two decades, quantum mechanical (QM) and combined quantum and molecular mechanical (QM/MM) calculations have proved to be useful tools in elucidating the reaction mechanisms of metalloproteins.[19-25] In particular, theoretical modelling can map the correspondence between conformational space and the energy landscape, and characterize the crucial points along the reaction coordinate, most notably the transition states.[26]

It is important to understand how the metal center and protein matrix separately contribute to the catalytic activity of the enzyme system. A proper approach to show catalytic power of enzymes is to compare the same reaction in the enzyme and solution. To highlight the effect of the metal center, results from the protein model are compared to the results from an active-site model containing only the oxophlorin without side chains and His as imidazole. To highlight the role of the protein in metal enzyme catalysis, we optimized QM/MM transition states and intermediates for the full reaction. Using the QM/MM methodology, we address several issues that cannot be considered with QM-cluster calculations. For example, we are interested in elucidating the effect of the protein environment on the reaction mechanism and the function of the hydrogen bond network in the distal pocket of HO.[16, 27, 28]

Methods

Density functional theory (DFT) calculations were employed, using the B3LYP functional as implemented in the Gaussian program series.[29] The structures were optimized with the 6-31+G* basis set and frequencies were calculated at the same level of theory. Local minima had only real frequencies, whereas the transition states had a single imaginary frequency. More accurate energies were calculated with the larger 6-311+G**basis set[30, 31] and they were corrected for with zero-point vibrational energies from the frequency calculations. The spin-unrestricted version of B3LYP (UB3LYP) method was used also for the singlet state when the reaction species were considered to have an open-shell singlet electronic configuration.[32-36] Atomic charge and spin densities were obtained by Mulliken calculations and natural bond orbital (NBO) analysis was used to characterize the electron distribution in the *d* orbitals of iron and the macrocycle ring, as well as to assign atomic charges.

The molecular-orbital analyses were performed by the Gauss View software, applied to the Gaussian output files. The QM region used for the QM-cluster calculations consisted of 53 or 54 atoms, viz. oxophlorin (without side chains) with imidazole and CO or H_2O as an axial ligand.

The QM/MM calculations were carried out with the program ComQum,[37-39] which is a combination of the QM software Turbomole[40] and the MM software Amber.[41] With ComQum, the protein and solvent are divided into two subsystems. System 1 is represented by a wave function and is optimized during the QM/MM calculations, whereas the remainder of the protein (system 2) is treated at MM level. It is represented as a set of atomic MM charges in the QM calculations. Thereby, the quantum chemical system is polarized by surroundings in a self-consistent way (electrostatic embedding). When there is a bond between the quantum and classical regions (a junction), the link-atom approach is applied,[42, 43] i.e. the QM system is truncated by hydrogen atoms, the positions of which are linearly related to the corresponding carbon atom in the protein.[37]

The QM system is similar to the one used in our previous work:[13] It is shown in Scheme 3 and consisted of oxophlorin (including all side chains) with H_2O as the sixth ligand and its proximal ligand His25 (modeled as methylimidazole), the distal residues Arg127 (modeled as $CH_3NHC(NH_2)_2^+$) and Asp131 (modeled as CH_3COO^-) and six crystal water molecules. This gives a total of 126 atoms in system 1. System 2 consisted of the remainder protein together with a surrounding sphere of water molecules, in total over 24 000 atoms.

The protein was set up as in our previous study.[30] The calculations were based on the X-ray structure of human HO-1 in complex with heme at 1.5 Å resolutions (PDB entry 1N45)[44]. All Arg and Lys residues were protonated and positively charged, whereas all Asp and Glu residues were deprotonated and negatively charged. His25 was protonated on the $N^{\delta 1}$ atom, His56, 132 and 223 were protonated on the $N^{\varepsilon 2}$ atom and the remaining His residues (all solvent-exposed) were doubly protonated. The total charge of the simulated system was –2. All crystal-water molecules were kept in the calculations and a sphere of solvation water molecules were added by the tleap module of the Amber software. The positions of all the added protons and water molecules were optimized by a 1-ns simulated annealing calculation, increasing the temperature to 370 K, followed by a minimization.

Scheme 3. The QM region used in the QM/MM calculations.

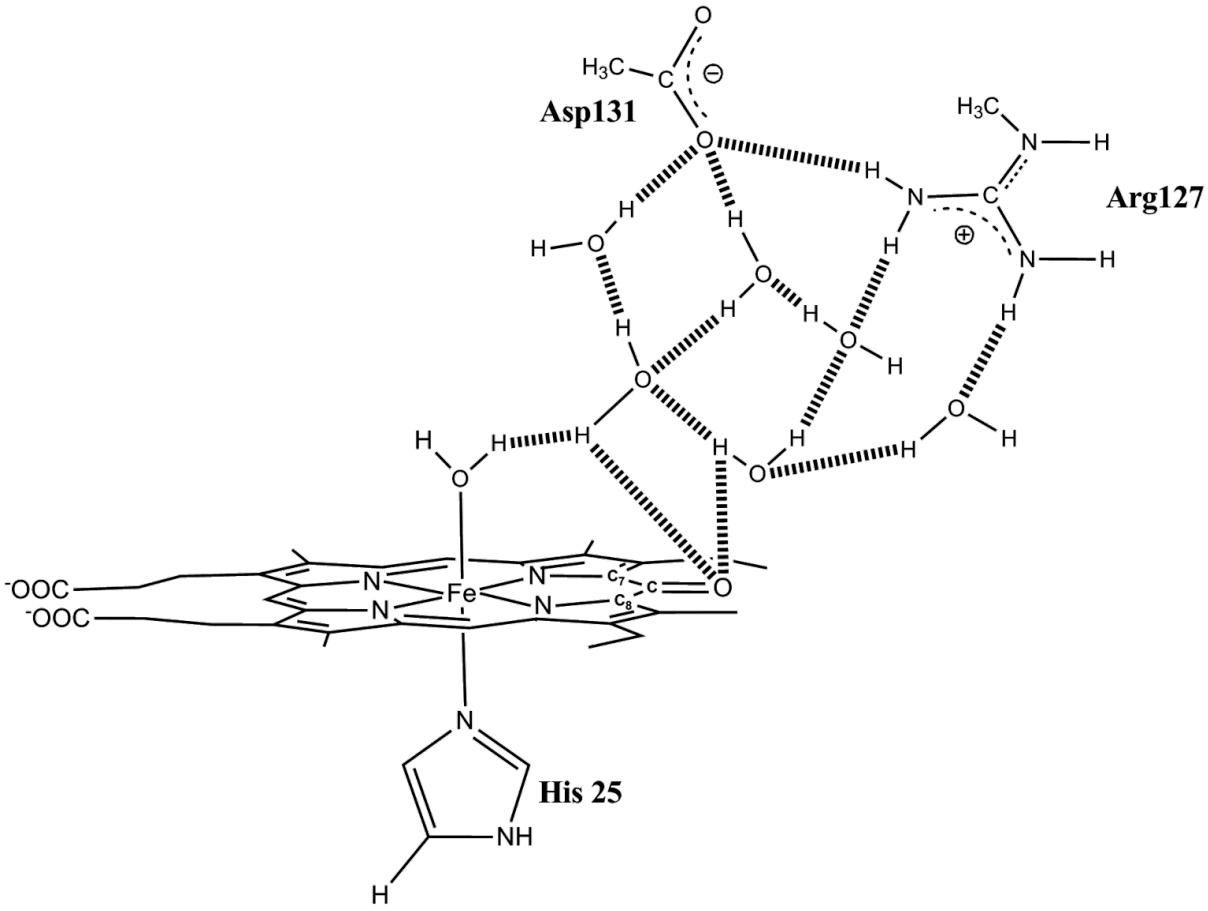

The total QMMM energy is calculated as

$$E_{QM/MM} = E_{QM} + E_{MM12} - E_{MM1} \qquad (1),$$

Where E_{QM} is the QM energy of quantum system truncated by hydrogen atoms, including the interaction between system 1 and the surrounding point charges. E_{MM1} is the MM energy of the quantum system, still truncated by hydrogen atoms, but without any electrostatic interactions, and E_{MM12} is the MM energy of the all the atoms in the system with carbon atoms at the junctions and with the charges of QM region zeroed, to avoid double counting at the electrostatic interaction. By this approach, errors caused by the truncation of QM system should cancel.

The QM calculations were carried out using the TPSS functional[45] with the Turbomole package[40]. The def2-SV(P) basis set[46, 47] was used for all atoms in the geometry optimizations. Dispersion effects were treated by the DFT-D3 approach and Becke–Johnson damping.[48] More accurate energies were obtained with single-point energy calculations with the def2-TZVP and def2-QZVP basis sets[49] (still with TPSS-D3), and with the B3LYP-D3 method[50, 51] and the def2-TZVP basis set. All single-point calculations were done with a point-charge model of the surroundings. All QM calculations were sped up by expanding the Coulomb interactions in an auxiliary basis set, the resolution-of-identity approximation.[49, 52]

To get energies that are converged with respect to the size of the QM system, big-QM calculations[53],[54] were performed using a QM system including all group within 6 Å of oxophlorin without side chains, the axial ligand and the imidazole group of His25, the backbone of residues 23–27 and all buried charged group in the protein (Arg127 and Asp131).[30]The calculations were performed at the TPSS/def2-SV(P) level of theory. To the big-QM energy, we added a standard MM correction for this big QM system and also a DFT-D3 dispersion correction with Becke–Johnson damping,[43] third-order terms and default parameters for the TPSS functional:[55]

$$E_{bq} = E_{big\text{-}QM} + E_{MM12} - E_{MM1} + E_{disp} \qquad (2)$$

Finally, the energies were extrapolated to the larger basis set and the B3LYP functional with single-point energy calculations for the QM system with the point-charge model:

$$E_{tot} = E_{bq} + E_{TPSS/QZ} - E_{TPSS/SV} + E_{B3LYP/TZ} - E_{TPSS/TZ} \qquad (3)$$

Result and Discussion

QM-cluster calculations

In this investigation, we started from [(Im)(CO)Fe^{II}($PO^{\bullet}$)] (**1**), where $PO^{\bullet}$ is the ring system of oxophlorin and imidazole (Im) and CO are axial ligands (Scheme 4). Our previous calculations[14] showed that the quartet and quintet structures (^{4}**1** and ^{6}**1**) are 20 and 15 kcal/mol higher in energy than the doublet spin ground state (^{2}**1**), respectively. Therefore, the quartet and sextet spin state surfaces are not expected to play any role in the reaction mechanism and we will focus on the doublet spin mechanism only. This result is in accordance with EPR data, which shows that binding of CO enhances the neutral Fe(II) keto π-radical component that can react with molecular oxygen.[56]

Scheme 4

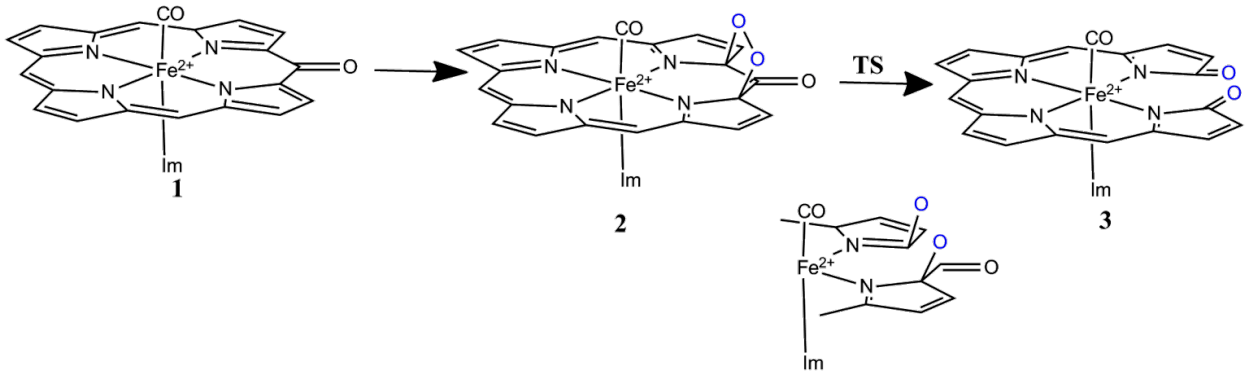

Hence, we investigated the mechanism in Scheme 5 for the oxidation of [(Im)(CO)Fe^{II}($PO^{\bullet}$)]In this path, the iron ion is six-coordinate throughout the mechanism with a non-reacting ligand. Therefore, O_2 cannot bind to Fe and it was instead placed on top of the oxophlorin ring. The highest positive charge and spin density of oxophlorin is found on the carbon atoms adjacent to the keto group of the oxophlorin and O_2 directly attacks these two carbon atoms to form the five-member intermediate (**2**)without any transition state. Subsequently, the O–O bond breaks via a **TS**

(characterized by an imaginary frequency of 425 cm^{-1}) to form the iron biliverdin complex [(Im)(CO)Fe^{III}(BV)] (**3**). Figure 1 shows the computed energy profile for these reactions. The first step (**1**→**2**) was uphill by 10 kcal/mol, whereas the ring-opening process (**2**→**3**) was exothermic by –45 kcal/mol with a small kinetic barrier of 7 kcal/mol (decreasing to 3 kcal/mol with a dielectric constant of ε = 25). The small energy barrier suggests that this pathway for the conversion of oxophlorin to biliverdin should be fast.

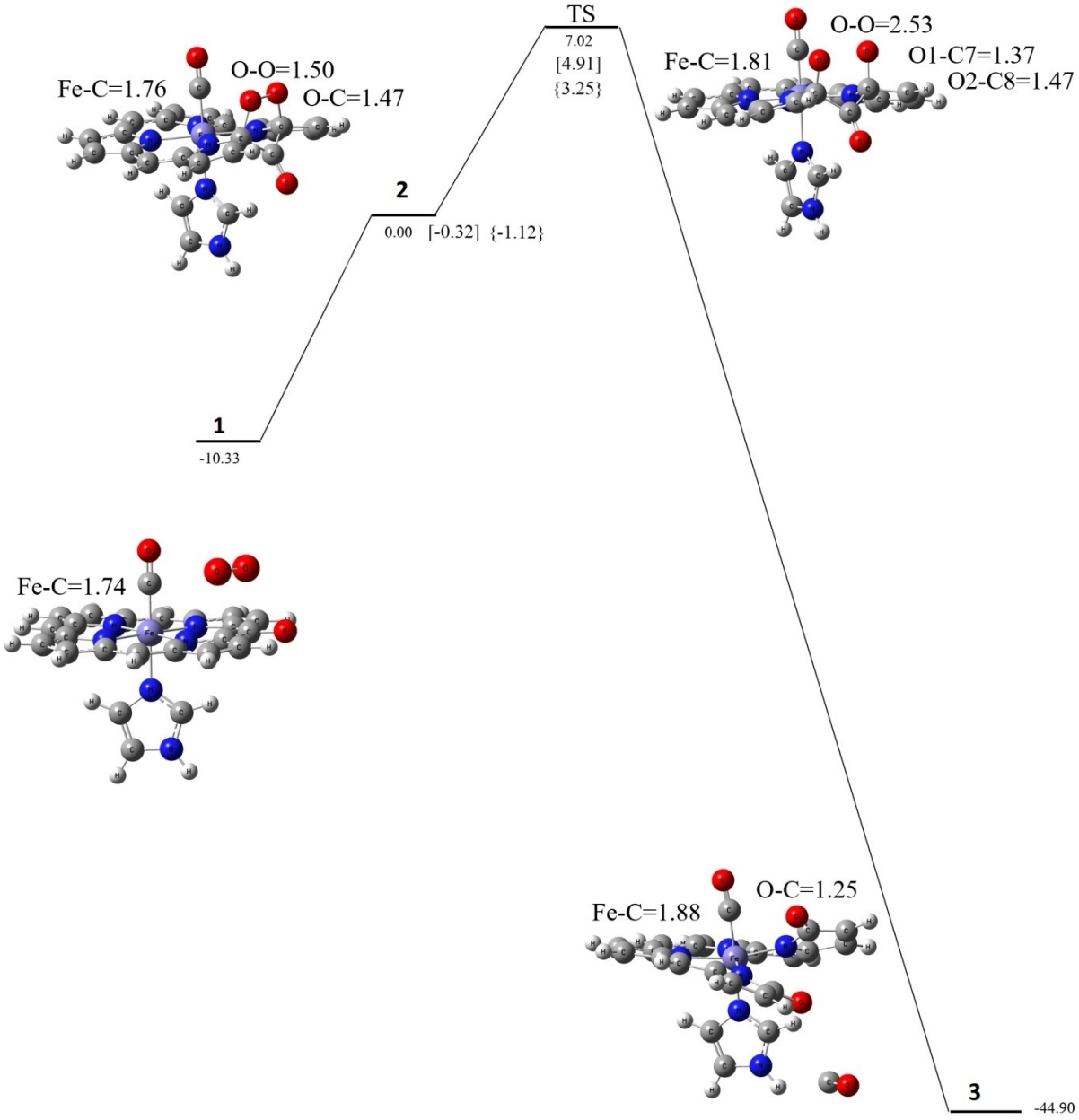

Figure 1. Potential energy landscape for conversion of **1** to **3** with CO as the axial ligand in the QM-cluster calculations. Data in square brackets corrected for a solvent with a dielectric constant of ε = 5.7, while data in curly brackets refers to a solvent with a dielectric constant of ε = 24.55. (all energies are in kcal/mol)

The direct attack of the O_2on the edge of oxophlorin is a pericyclic cycloaddition reaction, because two σ bonds form simultaneously. The HOMO of O_2, which has π* character, attacks the LUMO of the ring of **1**, which also has π* character, as can be seen in Figure 2.They form two new σ bonds between C7 and O1 and between C8 and O2. It can be seen from the figure that the lobes on C7 andO1 have the same sign, as do those onC8 with O2. There is no barrier to the concerted formation of the two C–O bonds, making the stepwise formation of intermediate **2** possible without any transition state.

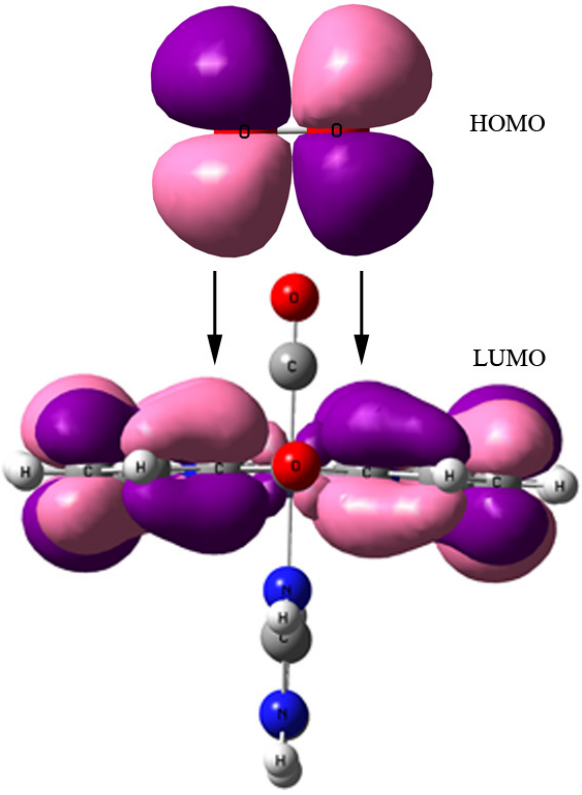

Figure 2.HOMO and LUMO Kohn−Sham orbitals for the interaction of O_2 with oxophlorin.

The calculated spins show that in species **2**, the spin density on the iron is 0.24 and that on O–O and tetrapyrrole ligand is 0.75. This electronic distribution is in accordance with the metal orbital

splitting shown in Figure 3.In the conversion of **2** to **3**, an intermolecular electron transfer occurs from the doubly occupied π_{xz} orbital to a singly occupied $\varphi_{ring+OO}$. The electron distribution in $\varphi_{ring+OO}$ has a σ^* character located in the O–O bond and a π^* character located in the tetrapyrrole ring. Because of this charge transfer from Fe(II) into the O–O σ^* bond, the latter is weakened and finally is cleaved. Due to the decrease in the occupation of the Fe π_{xz} orbital (doubly occupied in **2**but singly occupied in **3**),the axial Fe–CO bond length is elongated from1.76 Å in **2** to 1.88 Å in **3**.The charge transfer also led the charge density on Fe to increase from 1.23 in **2** to1.37 in **3**(the spin density on the iron is 0.87, and that on the biliverdin macrocycle is 0.12).To confirm the electronic configurations, NBO analysis for **2** and **3** are presented in Table 1. In species **2**, the occupancies of the α spin orbital for iron is 2.95 and that of the β spin orbital for iron is 2.71, which results in a net α spin of 0.24 on iron. Almost one unpaired electron with α spin is present on the macrocycle to make the whole system an iron(II) d^6 with the macrocycle as a dianionic radical. For species **3**, in iron the occupancy number of α spin orbitals is 2.76 and that of the β spin orbitals is 1.89, which results in a net α spin of 0.87 on the iron, showing that the whole system is Fe(III) d^5.

Table 1. NBO Analysis of the Electron Distribution of the Iron Atom of**2** and**3.**

***α* spin orbital**		***β* spin orbital**	
Occupancy	**Orbital**	**Occupancy**	**Orbital**
2			
0.99	LP (1)Fe	-0.96	LP (1)Fe
0.98	LP (2)Fe	-0.93	LP (2)Fe
0.98	LP (3)Fe	-0.81	LP (3)Fe
Sum of the***α*** spin electrons		Sum of the ***β*** spin electrons	
2.95		-2.71	
3			
0.97	LP (1)Fe	-0.97	LP (1)Fe
0.95	LP (2)Fe	-0.92	LP (2)Fe
0.84	LP (3)Fe		
Sum of the***α*** spin electron		Sum of the ***β*** spin electron	
2.76		-1.89	

In this pathway, iron biliverdin is formed by an irreversible extrusion of carbon monoxide from the unstable intermediate **2**. Such are action is known as cheletropic extrusion[57] because a small stable molecule (CO) dissociates in the reaction.

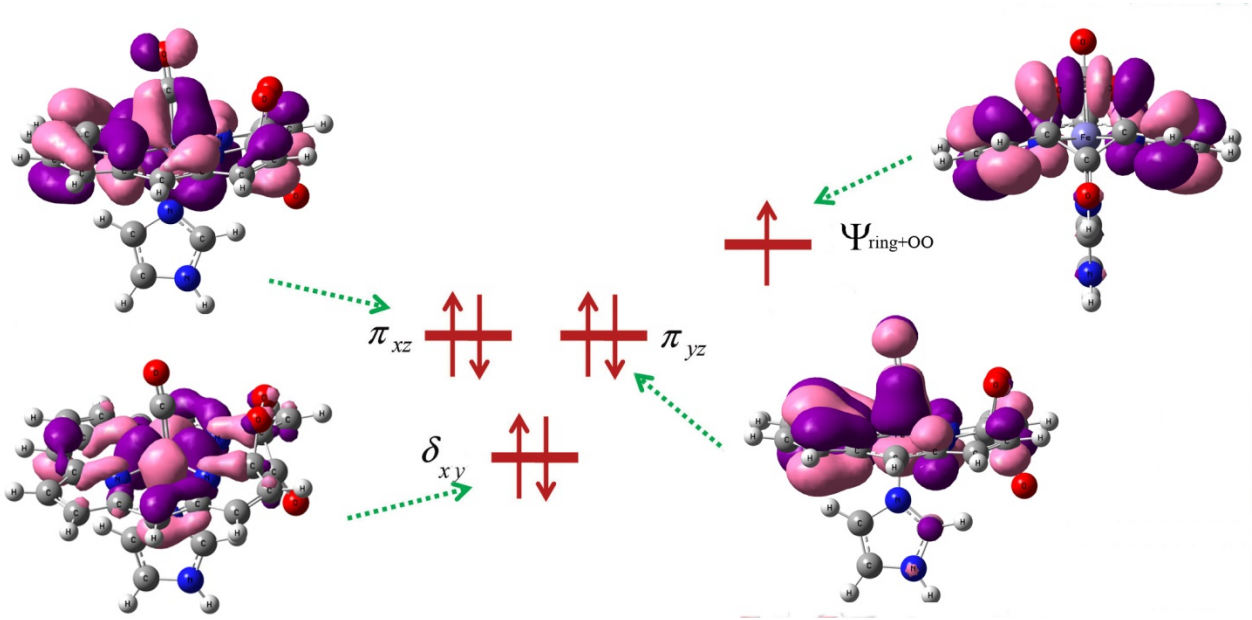

Figure 3. Kohn−Sham orbitals for the last four HOMOs of intermediate **2**

For the corresponding reaction with H_2O as the axial ligand, the ring opening process (**2**→**3**) was exothermic by –85 kcal/mol with a kinetic barrier of 5 kcal/mol. Again, the small energy barrier suggests that this pathway for the conversion of oxophlorin to biliverdin is a possible route. In the QM-cluster calculations for five-coordinated oxophlorin, the path that formed verdoheme was exothermic by 14.5 kcal/mol with a rate-determining barrier of 12 kcal/mol in the gas phase and the barrier decreased to 5–9 kcal/mol in solution, which are well in the range for enzymatic processes.

QM/MM calculations

To investigate the enzyme effect on the reaction, we also studied it with the QM/MM technique at the TPSS-D3/def2-SV(P) level of theory. The reaction was studied with three different axial ligands (CO, O_2 and H_2O) of Fe. The calculations were started from [(Im)(L)(Fe(II))(PO)] (**1**), for

which the doublet spin state was found to be the most stable species. The results are compared in Figure 4.

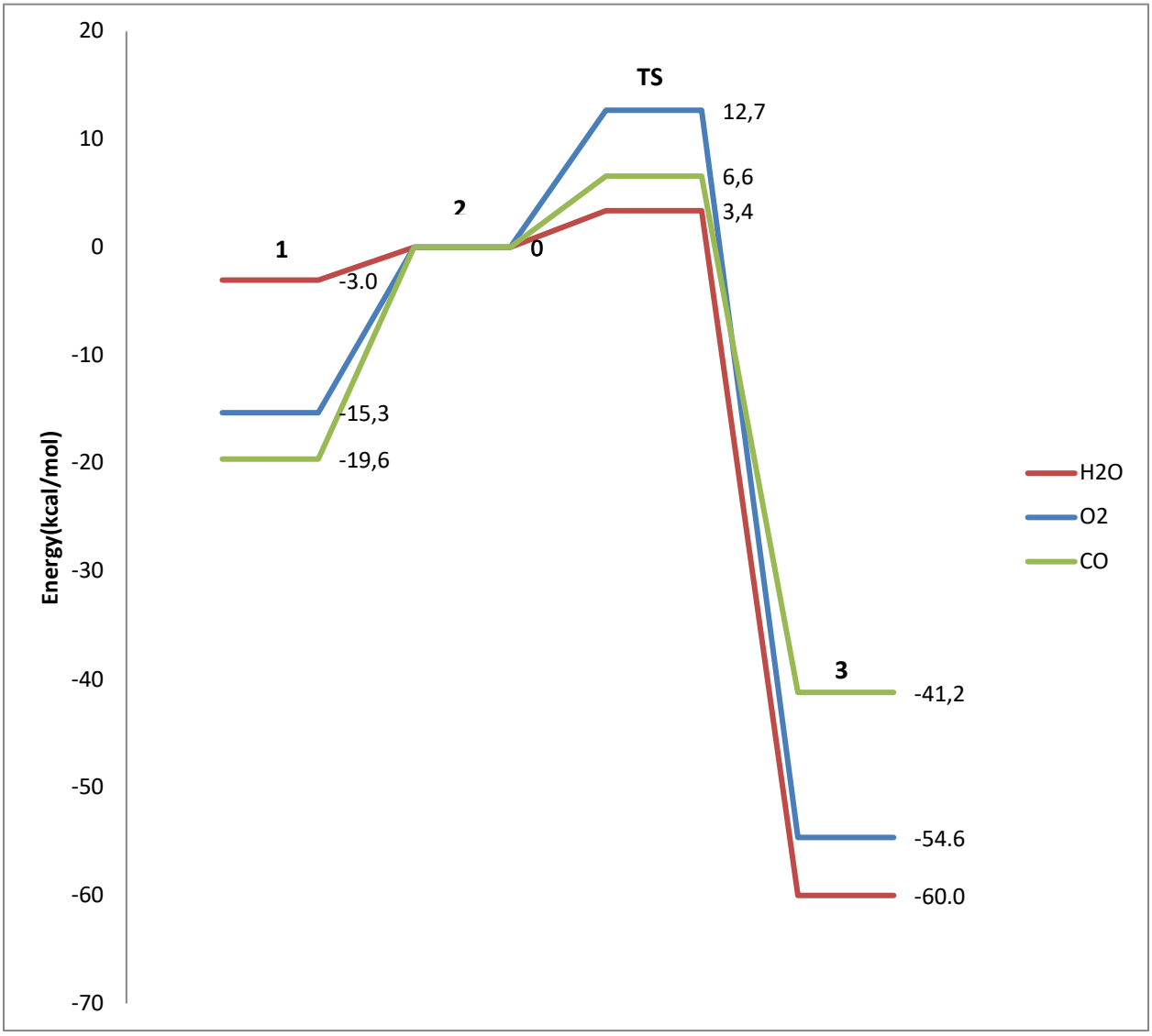

Figure 4. Relative energies in the reaction mechanism for the conversion of oxophlorin to biliverdin in the QM/MM calculations (obtained at the TPSS-D3-def2-SV(P) level of theory).

It can be seen that the reaction with a water ligand has the lowest activation energy (3 kcal/mol) and is also has the most exothermic reaction energy (60 kcal/mol). The energy for the first reaction (**1**→**2**) is also lowest, 3 kcal/mol. The two barriers are quite similar to what was found in the QM-cluster calculations, whereas the reaction energy is somewhat less exothermic (85 kcal/mol in the QM-cluster calculations). With the other two ligands, the barriers are higher (20 and 7 kcal/mol for CO and 15 and 13 kcal/mol for O_2) and the reaction energy is less exothermic (41 and 55 kcal/mol for CO and O_2, respectively).The binding energy of the three axial ligands follow the order CO>O_2>H_2O, which is the same in our previous QM-cluster calculations.[18] The barriers are very similar for QM and QM/MM, indicating that the surrounding enzyme has little influence on the energies.

As the results shown above indicate, the path with water ligand has the lowest transition state energy and is the most favored route energetically and thus was chosen to explore the mechanism. As one can see, the energy gap between structures 1 and 2 for the H_2O ligand is lower in QM/MM calculations while all other species like TS and product are more stable than for the other ligands in this pathway.

Optimized QM/MM structures of all intermediates in the reaction mechanism with H_2O as the axial ligand are shown in Figure 5 (the corresponding structures with CO and O_2as the axial ligand are given in the SI). It can be seen that the water cluster forms strong hydrogen bonds for all intermediates (shown as green dashed lines in Figure 5). In particular, there is a strong hydrogen bond between water as ligand and the O_2 molecule with waters cluster.

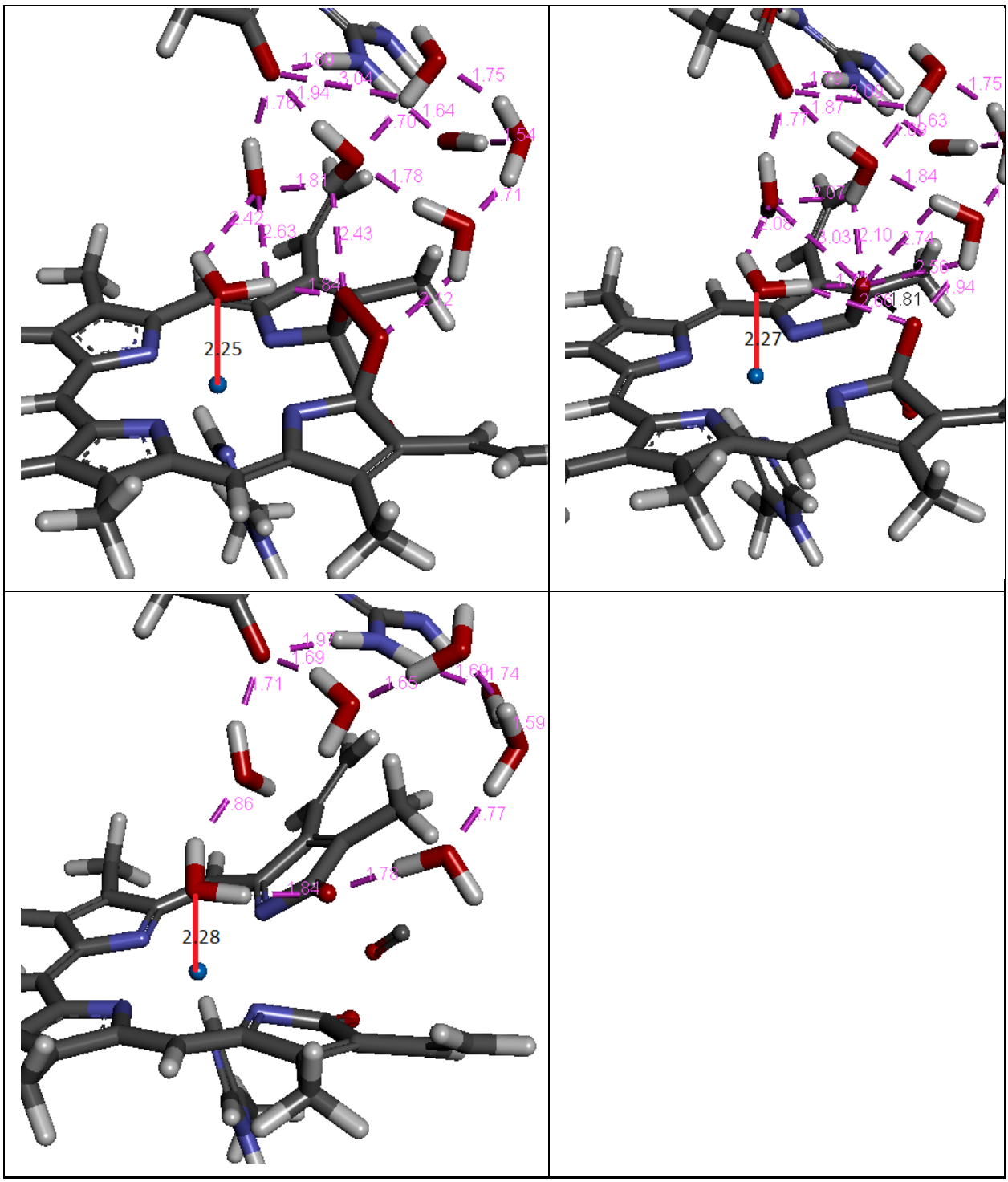

Figure 5. QM/MM optimized structure of the various intermediates in the suggested mechanism

Table 2. Selected distances throughout the reaction mechanism for water ligand in the QM-cluster and QM/MM calculations (first and second number, respectively).

QM/QMMM	O1-O2	C7-C	C8-C	C-O
2	1.55/1.53	1.54/1.54	1.53/1.52	1.21/1.21
TS	1.70/1.81	1.55/1.79	1.53/1.52	1.21/1.19
3	3.10/2.94	4.21/2.89	4.70/3.91	1.13/1.14

In Table 2, differences in the key distances between the QM/MM and QM-cluster calculations are shown. It can be seen that the most significant differences are that the O1–O2 and C7–C bonds are longer in the QM/MM calculations of **TS** (both 1.8 Å, compared to 1.7 and 1.5 Å in the QM-cluster calculations). Thus, there is a larger change when going from **2** to **TS** in the QM/MM calculations. The differences are even larger for the product (**3**), for which the QM/MM calculations give much shorter O1–O2 and C6–C bonds (3.0 and 2.9 Å) compared to the QM-cluster calculations(3.1 and 4.2 Å). This reflects the larger restrictions in the enzyme active site and they may explain why the reaction is less exothermic in the protein.

The energies in Figure 4 were obtained with QM/MM at the TPSS-D3/def2-SV(P) level of theory. More accurate energies were obtained by the big-QM approach using very large QM regions of almost 1000 atoms. Moreover, we also tested the B3LYP-D3 method and extrapolated the energies to the def2-QZVP basis set. The various energies are listed in Table S1. It can be seen that the effect of increasing the basis set from def2-SV(P) to def2-QZVP is rather small, 1 and –5 kcal/mol for the activation and reaction energy, respectively. The effect of the functional is larger, 2 and –9 kcal/mol. The difference between the QM/MM and big-QM energies is modest, 3 and 0 kcal/mol, respectively. Summing up all energies according to Eqn. 3 gives our final energy estimate E_{tot}.

It indicates that the reaction is exothermic by –74 kcal/mol, with an activation barrier of 9 kcal/mol. Both are higher than in the QM-cluster calculations by 11 and 4 kcal/mol, respectively. Thus, the results indicate that the conversion of oxophlorin to biliverdin should be very fast and it is a feasible route. The barrier was low also in the QM-cluster model, showing that the main catalytic effect comes from the metal center, whereas the role of protein is probably to control the specificity of the reaction (towards the α-meso carbon in the first reaction step).

In our recent article,[13] we studied the formation of verdoheme from five-coordinated oxophlorin with the same approach (QM/MM structures and big-QM energies extrapolated to the B3LYP-D3/def2-QZVP level). The results indicated that the reaction is exothermic by 35 kcal/mol with a activation barrier of 19 kcal/mol. Comparison with the present results, suggests that the direct formation of biliverdin should be faster than verdoheme generation, provided that the formation of six-coordinate oxophlorin is fast enough. This is supported by experimental evidence, indicating that verdoheme yield does not exceed 50%.[15]

Conclusions

A new enzymatic mechanism has been proposed, which indicates that verdoheme and biliverdin can be formed simultaneously. This is in good agreement with experimental results.[15] If oxophlorin is six-coordinated oxophlorin, O_2may directly attack the carbon atoms adjacent to the keto group of the oxophlorin to form a five-member ring structure. Subsequently, the O–O bond is cleaved via a transition state to form the iron biliverdin complex. If oxophlorin instead is five-coordinated, O_2 is predicted to coordinate to Fe and the terminal oxygen atom can attack the carbon atom adjacent to keto group of oxophlorin, followed by a hemolytic cleavage of O_2 and an attack of the same oxygen atom also on the other carbon adjacent to keto group of oxophlorin, which leads to the release of carbon monoxide and the formation of verdoheme. This reaction was considered in our previous study.[13, 14]

The ring opening mechanism from oxophlorin to biliverdin has been investigated for three Fe ligands CO, O_2 and H_2O by QM/MM calculations at the TPSS-D3/def2-SV(P) level and at the B3LYP/6-311+G** level in QM-cluster calculations. The QM/MM results were then improved by big-QM calculations using a very large QM region of almost 1000 atoms and the energies were extrapolated to theB3LYP-D3 method and the def2-QZVP basis set. In the QM-cluster calculations, the H_2O ligand has the lowest barrier (5 kcal/mol), and the reaction was exothermic by 85 kcal/mol. In the QM/MM calculations, the barrier was slightly higher, 9 kcal/mol and the exothermicity was slightly lower, 74 kcal/mol. The results suggest that the main catalytic effect comes from the metal center, whereas the protein controls the specificity of the reaction.

Acknowledgment

This investigation has been supported by grants from the research council of Shahid Beheshti University and the Swedish research council (project 2014-5540). The computations were performed on computer resources provided by the Swedish National Infrastructure for Computing (SNIC) at Lunarc at Lund University and HPC2N at Umeå University.

Abbreviations

DFT, density functional theory; HO, heme oxygenase; QM, quantum mechanics; QM/MM, quantum mechanics/molecular mechanics.

AUTHOR INFORMATION

Corresponding Authors

*E-mail: m-zahedi@sbu.ac.ir , Phone: +98-21-29902889.

n-safari@sbu.ac.ir, Phone: +98-21-29902886.

Reference

1. M. Sono, M. P. Roach, E. D. Coulter and J. H. Dawson, *Chem. Rev.*, 1996, **96**, 2841-2888.
2. P. R. Ortiz de Montellano, *Acc. Chem. Res.*, 1998, **31**, 543-549.
3. P. R. O. de Montellano and A. Wilks, *Adv. Inorg. Chem.*, 2000, **51**, 359-407.

4. C. Colas and P. R. Ortiz de Montellano, *Chem. Rev.*, 2003, **103**, 2305-2332.
5. M. Unno, T. Matsui and M. Ikeda-Saito, *Nat. Prod. Rep.*, 2007, **24**, 553-570.
6. T. Matsui, M. Unno and M. Ikeda-Saito, *Acc. Chem. Res.*, 2009, **43**, 240-247.
7. A. Wilks, *Antioxid. Redox Signaling*, 2002, **4**, 603-614.
8. D. Kumar, S. P. de Visser and S. Shaik, *J. Am. Chem. Soc.*, 2005, **127**, 8204-8213.
9. A. L. Balch, *Coord. Chem. Rev.*, 2000, **200**, 349-377.
10. W. Lai, H. Chen, T. Matsui, K. Omori, M. Unno, M. Ikeda-Saito and S. Shaik, *J. Am. Chem. Soc.*, 2010, **132**, 12960-12970.
11. R. Tenhunen, H. Marver, N. Pinstone, W. Trager, D. Y. Cooper and R. Schmid, *Biochemistry*, 1972, **11**, 1716-1720.
12. J. C. Docherty, B. A. Schacter, G. D. Firneisz and S. Brown, *J. Biol. Chem.*, 1984, **259**, 13066-13069.
13. F. S. Alavi, M. Zahedi, N. Safari and U. Ryde, *J. Phys. Chem. B*, 2017.
14. M. Gheidi, N. Safari and M. Zahedi, *Dalton Trans.*, 2017.
15. A. L. Balch, L. Latos-Grazynski, B. C. Noll, M. M. Olmstead and N. Safari, *J. Am. Chem. Soc.*, 1993, **115**, 9056-9061.
16. H. Chen, Y. Moreau, E. Derat and S. Shaik, *J. Am. Chem. Soc.*, 2008, **130**, 1953-1965.
17. M. Gheidi, N. Safari and M. Zahedi, *Inorg. Chem.*, 2012, **51**, 7094-7102.
18. M. Gheidi, N. Safari and M. Zahedi, *Inorg. Chem.*, 2014, **53**, 2766-2775.
19. H. M. Senn and W. Thiel, *Angew. Chem., Int. Ed.*, 2009, **48**, 1198-1229.
20. S. C. Kamerlin, M. Haranczyk and A. Warshel, *J. Phys. Chem. B*, 2008, **113**, 1253-1272.
21. P. E. Siegbahn and F. Himo, *JBIC, J. Biol. Inorg. Chem.*, 2009, **14**, 643-651.
22. H. Hu and W. Yang, *Annu. Rev. Phys. Chem.*, 2008, **59**, 573-601.
23. U. Ryde, *Curr. Opin. Chem. Biol.*, 2003, **7**, 136-142.
24. B. Kirchner, F. Wennmohs, S. Ye and F. Neese, *Curr. Opin. Chem. Biol.*, 2007, **11**, 134-141.
25. F. Neese, *Coord. Chem. Rev.*, 2009, **253**, 526-563.
26. E. Polymeropoulos, *Berichte der Bunsengesellschaft für physikalische Chemie*, 1992, **96**, 1323-1324.
27. T. Matsui, M. Furukawa, M. Unno, T. Tomita and M. Ikeda-Saito, *J. Biol. Chem.*, 2005, **280**, 2981-2989.
28. J. C. Rodríguez, Y. Zeng, A. Wilks and M. Rivera, *J. Am. Chem. Soc.*, 2007, **129**, 11730-11742.
29. M. Frisch, G. Trucks, H. Schlegel, G. Scuseria, M. Robb, J. Cheeseman, J. Montgomery Jr, T. Vreven, K. Kudin and J. Burant, *Google Scholar*.
30. M. Swart, *J. Chem. Theory Comput.*, 2008, **4**, 2057-2066.
31. C. J. Cramer, *Essentials of computational chemistry: theories and models*, John Wiley & Sons, 2013.
32. C. Lee, W. Yang and R. G. Parr, *Phys. Rev. B*, 1988, **37**, 785.
33. S. H. Vosko, L. Wilk and M. Nusair, *Can. J. Phys.*, 1980, **58**, 1200-1211.
34. P. Stephens, F. Devlin, C. Chabalowski and M. J. Frisch, *J. Phys. Chem.*, 1994, **98**, 11623-11627.
35. T. Yoshinaga, Y. Sudo and S. Sano, *Biochem. J.*, 1990, **270**, 659-664.
36. Y. Shiota and K. Yoshizawa, *J. Am. Chem. Soc.*, 2000, **122**, 12317-12326.
37. U. Ryde, *J. Comput.-Aided Mol. Des.*, 1996, **10**, 153-164.
38. U. Ryde and M. H. Olsson, *Int. J. Quantum Chem.*, 2001, **81**, 335-347.
39. U. Ryde, L. Olsen and K. Nilsson, *J. Comput. Chem.*, 2002, **23**, 1058-1070.
40. O. Treutler and R. Ahlrichs, *J. Chem. Phys.*, 1995, **102**, 346-354.
41. D. Case, T. Darden, T. Cheatham III, C. Simmerling, J. Wang, R. Duke, R. Luo, M. Crowley, R. Walker and W. Zhang, *There is no corresponding record for this reference*, 2005.
42. P. E. Siegbahn and M. R. Blomberg, *Annu. Rev. Phys. Chem.*, 1999, **50**, 221-249.

43. D. Lecerof, M. Fodje, A. Hansson, M. Hansson and S. Al-Karadaghi, *J. Mol. Biol.*, 2000, **297**, 221-232.
44. D. J. Schuller, Wilks, A., Ortiz de Montellano, P.R., Poulos, T.L., *Comparison of the Heme-free and -bound Crystal Structures of Human Heme Oxygenase-1*, http://www.rcsb.org/pdb/explore/explore.do?structureId=1N45.
45. J. Tao, J. P. Perdew, V. N. Staroverov and G. E. Scuseria, *Phys. Rev. Lett.*, 2003, **91**, 146401.
46. A. Schäfer, H. Horn and R. Ahlrichs, *J. Chem. Phys.*, 1992, **97**, 2571-2577.
47. F. Weigend and R. Ahlrichs, *Phys. Chem. Chem. Phys.*, 2005, **7**, 3297-3305.
48. S. Grimme, S. Ehrlich and L. Goerigk, *J. Comput. Chem.*, 2011, **32**, 1456-1465.
49. K. Eichkorn, O. Treutler, H. Öhm, M. Häser and R. Ahlrichs, *Chem. Phys. Lett.*, 1995, **240**, 283-290.
50. A. D. Becke, *J. Chem. Phys.*, 1993, **98**, 5648-5652.
51. R. H. Hertwig and W. Koch, *Chem. Phys. Lett.*, 1997, **268**, 345-351.
52. K. Eichkorn, F. Weigend, O. Treutler and R. Ahlrichs, *Theor. Chem. Acc.*, 1997, **97**, 119-124.
53. L. Hu, P. r. Söderhjelm and U. Ryde, *J. Chem. Theory Comput.*, 2011, **7**, 761-777.
54. S. Sumner, P. r. Söderhjelm and U. Ryde, *J. Chem. Theory Comput.*, 2013, **9**, 4205-4214.
55. S. Grimme, *J. Comput. Chem.*, 2004, **25**, 1463-1473.
56. Y. Liu, P. Moënne-Loccoz, T. M. Loehr and P. R. O. de Montellano, *J. Biol. Chem.*, 1997, **272**, 6909-6917.
57. G. Y. Wooi and J. M. White, *Org. Biomol. Chem.*, 2005, **3**, 972-974.